Available online at www.sciencedirect.com
ScienceDirect
Materials Research Bulletin 43 (2008) 1307–1320
Materials Research Bulletin
www.elsevier.com/locate/matresbu

Structural characterization, thermal, spectroscopic and magnetic studies of the $(C_3H_{12}N_2)_{0.75}[Mn_{1.50}{}^{II}Fe_{1.50}{}^{III}(AsO_4)F_6]$ and $(C_3H_{12}N_2)_{0.75}[Co_{1.50}{}^{II}Fe_{1.50}{}^{III}(AsO_4)F_6]$ compounds

B. Bazán [a], J.L. Mesa [b,*], A. Peña [b], E. Legarra [c], J.L. Pizarro [a], M.I. Arriortua [a], T. Rojo [b]

[a] Departamento de Mineralogía y Petrología, Universidad del País Vasco/EHU, Apdo. 644, E-48080 Bilbao, Spain
[b] Departamento de Química Inorgánica, Universidad del País Vasco/EHU, Apdo. 644, E-48080 Bilbao, Spain
[c] Departamento de Física Aplicada II, Facultad de Ciencia y Tecnología, Universidad del País Vasco/EHU, Apdo. 644, E-48080 Bilbao, Spain

Received 9 March 2007; received in revised form 2 May 2007; accepted 4 May 2007
Available online 13 May 2007

Abstract

The $(C_3H_{12}N_2)_{0.94}[Mn_{1.50}Fe_{1.50}{}^{III}(AsO_4)F_6]$ and $(C_3H_{12}N_2)_{0.75}[Co_{1.50}Fe_{1.50}{}^{III}(AsO_4)F_6]$ compounds **1** and **2** have been synthesized using mild hydrothermal conditions. These phases are isostructural with $(C_3H_{12}N_2)_{0.75}[Fe_{1.5}{}^{II}Fe_{1.5}{}^{III}(AsO_4)F_6]$. The compounds crystallize in the orthorhombic *Imam* space group. The unit cell parameters calculated by using the patterns matching routine of the FULPROOF program, starting from the cell parameters of the iron(II),(III) phase, are: $a = 7.727(1)$ Å, $b = 11.047(1)$ Å, $c = 13.412(1)$ Å for **1** and $a = 7.560(1)$ Å, $b = 11.012(1)$ Å, $c = 13.206(1)$ Å for **2**, being $Z = 8$ in both compounds. The crystal structure consists of a three-dimensional framework constructed from edge-sharing $[M^{II}(1)_2O_2F_8]$ (M = Mn, Co) dimeric octahedra linked to $[Fe^{III}(2)O_2F_4]$ octahedra through the F(1) anions and to the $[AsO_4]$ tetrahedra by the O(1) vertex. This network gives rise two kinds of chains, which are extended in perpendicular directions. Chain **1** is extended along the *a*-axis and chain **2** runs along the *c*-axis. These chains are linked by the F(1) and O(1) atoms and establish cavities delimited by eight or six polyhedra along the [1 0 0] and [0 0 1] directions, respectively. The propanediammonium cations are located inside these cavities. The thermal study indicates that the structures collapse with the calcination of the organic dication at 255 and 285 °C for **1** and **2**, respectively. The Mössbauer spectra in the paramagnetic state indicate the existence of two crystallographically independent positions for the iron(III) cations and a small proportion of this cation in the positions of the divalent Mn(II) and Co(II) ones. The IR spectrum shows the protonated bands of the H_2N– groups of the propanediamine molecule and the characteristic bands of the $[AsO_4]^{3-}$ arsenate oxoanions. In the diffuse reflectance spectra, it can be observed the bands characteristic of trivalent iron(III) cation and divalent Mn(II) and Co(II) ones in a distorted octahedral symmetry. The calculated Dq and B-Racah parameters for the cobalt(II) phase are 710 and 925 cm^{-1}, respectively. The ESR spectra of compound **1** maintain isotropic with variation in temperature, being $g = 1.99$. Magnetic measurements for both compounds indicate that the main magnetic interactions are antiferromagnetic in nature. However, at low temperatures small ferromagnetic components are detected, which are probably due to a spin decompensation of the two different metallic cations. The hysteresis loops give values of the remnant magnetization and coercive field of 84.5, 255 emu/mol and 0.01, 0.225 T for phases **1** and **2**, respectively.

Keywords: A. Microporous materials; C. Infrared spectroscopy; C. Mössbauer spectroscopy; C. Thermogravimetric analysis; C. X-ray diffraction; D. Electronic paramagnetic resonance; D. Magnetic properties

* Corresponding author. Tel.: +34 946015523; fax: +34 946013500.
E-mail addresses: joseluis.mesa@ehu.es, qipmeruj@lg.ehu.es (J.L. Mesa).

0025-5408/$ – see front matter © 2007 Published by Elsevier Ltd.
doi:10.1016/j.materresbull.2007.05.016

1. Introduction

The world of crystalline porous materials has long been dominated by aluminosilicates zeolites, which are widely used in catalysis, separations, and ion-exchange processes [1]. In the study of these materials, although the designing phases similar to aluminosilicates zeolitic structures has been the subject of main interest, the discovery of new compounds with novel structural features has also assumed an important role [2].

The incorporation of transition elements to the organically templated open-framework system is particularly fascinant due to the possibility of the variation in the coordination environment around the metal ion, as well as, the possibility of observing interesting magnetic properties [3]. Among these materials, iron phosphates occupy the first position because they have incremented a rich structural chemistry [4]. The open framework phosphates are sometimes synthesized hydrothermal employing fluoride ions, which are often incorporated as part of the framework and act as a bridge between the iron centers [5].

Arsenates are also interesting anions in comparison with phosphates to be used in the attainment of compounds with occluding organic amines. To date, many organically templated iron(III) arsenates are known [6], and also mixed valence iron(II,III) arsenates, which exhibit interesting magnetic properties [7]. However, the mixed valence cations arsenates are scarce.

In this study, we present the first three-dimensional compounds organically templated Mn(II)–Fe(III) and Co(II)–Fe(III) fluorinated arsenate with formula $(C_3H_{12}N_2)_{0.75}[Mn_{1.50}^{II}Fe_{1.50}^{III}(AsO_4)F_6]$ and $(C_3H_{12}N_2)_{0.75}[Co_{1.50}^{II}Fe_{1.12}^{III}(AsO_4)F_6]$, which have been synthesized using propanediammonium as structural directing agent. These compounds present interesting magnetic properties with a small ferromagnetic contribution at low temperatures due to the existence of a spin decompensation between the different metallic centers.

2. Experimental

2.1. Synthesis and characterization

The $(C_3H_{12}N_2)_{0.75}[Mn_{1.50}Fe_{1.50}^{III}(AsO_4)F_6]$ and $(C_3H_{12}N_2)_{0.75}[Co_{1.50}Fe_{1.50}^{III}(AsO_4)F_6]$ compounds **1** and **2** have been synthesized using mild hydrothermal conditions. The starting reagent were $As_2O_5{\cdot}3H_2O$ (3.7 mmol), $Fe_2(SO_4)_3{\cdot}5H_2O$ (0.25 mmol), $MnCl_2{\cdot}4H_2O$ (0.5 mmol) or $CoCl_2{\cdot}6H_2O$ (0.5 mmol), HF (57.5 mmol) and propanediamine (8.52 mmol) in a volume of *ca*. 30 mL of water. The initial pH of the reaction mixture was *ca*. 3. The syntheses were carried out in poly(tetrafluoroethylene)-lined stainless steel containers under autogeneous pressure, filled to *ca*. 75% volume capacity, and all reagents were stirred briefly before heating. The reaction mixture was heated at 170 °C for 5 days, followed by slow cooling to room temperature. The final pH of the reaction did not show significant variation with respect to that of the initial reagents. The resulting polycrystalline products were filtered off, washed with ether, and dried in air for 6 h.

The metal ions and arsenic contents were confirmed by inductively coupled plasma atomic emission spectroscopy (ICP-AES) analysis performed with a RL Fisons 3410 spectrometer. Fluorine content was determined using a fluorine selective electrode. C, H and N elemental analysis was carried out with a Perkin-Elmer Model 240 automatic analyser. Observed: Fe, 17.4; Mn, 17.1; As, 15.3; F, 23.5; C, 5.4; N, 4.2; H, 1.6. Calculated for **1**: Fe, 17.6; Mn, 17.3; As, 15.7; F, 23.9; C, 5.7; N, 4.4; H 1.9. Observed: Fe, 16.7; Co, 17.9; As, 15.1; F, 23.1; C, 5.5; N, 4.2; H, 1.8. Calculated for **2**: Fe, 17.4; Co, 18.3; As, 15.5; F, 23.6; C, 5.6; N, 4.3; H 1.9. The density, 2.71(1) and 2.88(2) g cm^{-3} for **1** and **2**, respectively, was measured by flotation in a mixture of CH_2I_2/CCl_4.

2.2. Thermal study

Thermogravimetric measurements were carried out heating the samples at 5 °C min^{-1} under air in the 30–800 °C temperature range using a SDC 2960 Simultaneous DSC-TGA TA instrument. Below 200 °C, the decomposition curves reveal a small loss of mass, approximately 2%, which can be attributed to the adsorbed water in the compound, or to the existence of water molecules in the cavities partially occupied by the propanediammonium cations. Between, 250 and 600 °C several superimposed mass losses are observed which are due to the simultaneous elimination of the propanediammonium cations and the fluoride anions. Above 650 °C, additional weight loss is not detected in the thermogravimetric curves. The X-ray patterns of the residues obtained from the thermogravimetric analysis show the

presence of peaks which can be indexed with the unit cell parameters of $Fe(AsO_4)$ [$P2_1/n$, $a = 5.012$ Å, $b = 8.081$ Å, $c = 7.568$ Å, $\beta = 104.46°$] [8a], Fe_2O_3 [$P4_132$, $a = 5.012$ Å] [8b], $Mn(AsO_4)$ [$P2_1/n$, $a = 6.683$ Å, $b = 8.930$ Å, $c = 4.791$ Å, $\beta = 93.813°$] [8c] and MnO_2 [$Pnam$, $a = 9.322$ Å, $b = 4.453$ Å, $c = 2.840$ Å, $\beta = 93.813°$] [8d] for **1** and $Fe(AsO_4)$ [$P2_1/n$, $a = 5.012$ Å, $b = 8.081$ Å, $c = 7.568$ Å, $\beta = 104.46°$] [8a], Fe_2O_3 [$P4_132$, $a = 5.012$ Å] [8b], $Co_3(AsO_4)_2$ [$P2_1/c$, $a = 6.457$ Å, $b = 8.509$ Å, $c = 11.186$ Å, $\beta = 90.730°$] [8e] and CoO [$Fm\bar{3}m$, $a = 4.261$ Å] [8f] for **2**.

The thermal behavior of compounds **1** and **2** has also been investigated by time-resolved X-ray thermodiffractometry. The patterns were collected in air using a PHILIPS X'PERT automatic diffractometer (Cu Kα radiation) equipped with a variable-temperature stage (Anton Paar HTK16) and a Pt sample holder. The data were recorded in 2θ steps of 0.02° in the range $5° \leq 2\theta \leq 50°$, counting for 1 s per step and increasing the temperature at 5 °C min^{-1} from room temperature up to 650 °C. The results are given in Fig. 1. The compounds are stable up to *ca.* 255 and 285 °C for **1** and **2**, respectively. In the 315–330 °C range the intensity of the peaks decrease dramatically for both phases. This result can be associated with the calcination of the organic dication and the elimination of the fluoride anions. From 330 °C and up to 600 °C for **1** and 585 °C for **2** no diffraction maxima are observed in the thermodiffractogram, indicating that the decomposition of the compounds gives amorphous phases. Above 600 °C the peaks belonging to the inorganic residues appear, and their composition is the same than that obtained in the thermogravimetric analysis.

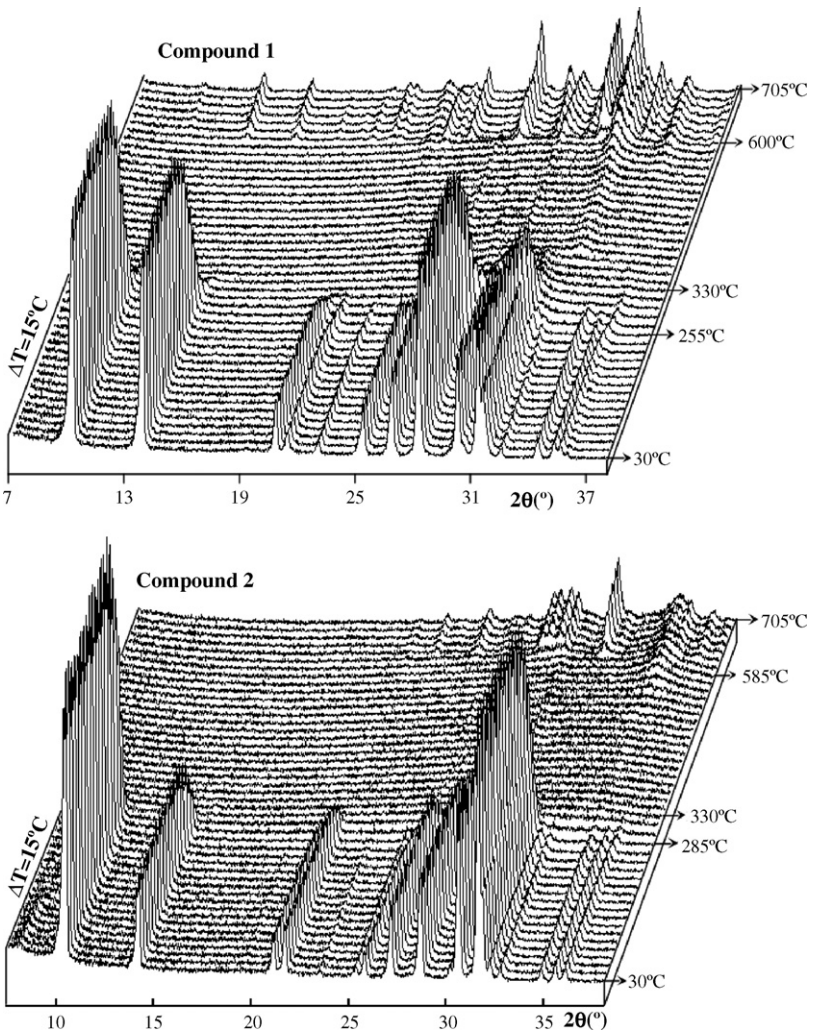

Fig. 1. Thermodiffractograms of compounds **1** and **2**.

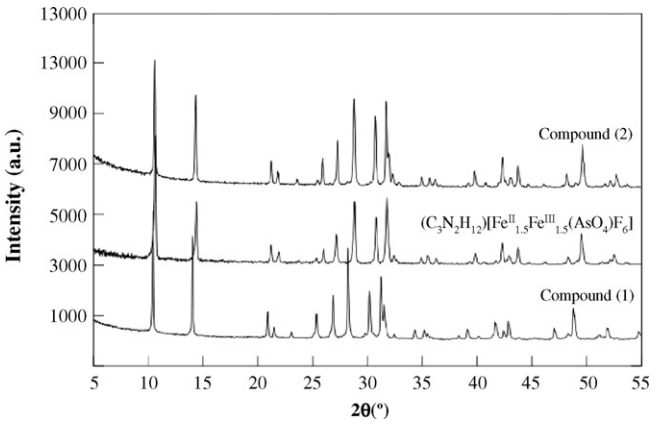

Fig. 2. X-ray powder diffraction patterns for the title compounds and for $(C_3H_{12}N_2)_{0.75}[Fe_{1.5}^{II}Fe_{1.5}^{III}(AsO_4)F_6]$.

2.3. X-ray powder diffraction study

The structural characterization of compounds **1** and **2** has been carried out from X-ray diffraction powder data. The intensities of the diffractograms have been recordered on a Philips X'Pert automatic diffractometer (Cu Kα radiation). The intensities have been measured in the 5–90° in 2θ, with step of 0.02° and 12 s per step.

Phases **1** and **2** are isostructural with $(C_3H_{12}N_2)_{0.75}[Fe_{1.5}^{II}Fe_{1.5}^{III}(AsO_4)F_6]$ [7], as can be seen from the diffractograms collected for the three compounds (Fig. 2). Attempts performed in order to refine the crystal structures of **1** and **2** starting from the atomic coordinates of the iron (II,III) phase and the intensities of their diffractograms were unsuccessful, due to the strong preferred orientation that show (**1**) and (**2**). So, the profile refinement of both phases **1** and **2** has been performed using the unit cell parameters of $(C_3H_{12}N_2)_{0.75}[Fe_{1.5}^{II}Fe_{1.5}^{III}(AsO_4)F_6]$ [7] in the *Imam* space group using the pattern matching routine of the FULLPROF program [9] (see Supplementary Material). The refined unit cell parameters obtained for **1** and **2** are $a = 7.727(1)$ Å, $b = 11.047(1)$ Å, $c = 13.412(1)$ Å for **1** and $a = 7.560(1)$ Å, $b = 11.012(1)$ Å, $c = 13.206(1)$ Å for **2**, respectively, being $Z = 8$ in both phases. These parameters are similar to those of $(C_3H_{12}N_2)_{0.75}[Fe_{1.5}^{II}Fe_{1.5}^{III}(AsO_4)F_6]$, $a = 7.566(2)$ Å, $b = 11.034(3)$ Å and $c = 13.233(5)$ Å [7].

2.4. Physical measurements

The IR spectra (KBr pellets) were obtained with a Mattson Satellite FTIR spectrophotometer in the 400–4000 cm^{-1} range. Diffuse reflectance spectra were registered at room temperature on a Cary 5000 spectrophotometer in the 210–2000 nm range. Mössbauer measurements were recorded at room temperature with a ^{57}CoRh source. ESR spectra were collected using a Bruker ESP 300 spectrometer, and an Oxford Instrument (ITC 4) regulator to stabilize the temperature. Magnetic measurements of powdered samples were carried out in the temperature range 5–300 K, using a Quantum Design MPMS-7 SQUID magnetometer. The magnetic fields were 0.1, 0.05 and 0.01 T, these values lie within the range of linear dependence of magnetization *versus* magnetic field, even a 5.0 K.

3. Results and discussion

3.1. Structural description

The crystal structure of phases **1** and **2** consists of a three-dimensional framework which is formed by O(1)–O(1) edge-sharing $[M^{II}(1)_2O_2F_8]$ (M = Mn, Co) dimeric octahedra linked to $[Fe^{III}(2)O_2F_4]$ octahedra through the F(1) anions and to the $[AsO_4]$ tetrahedra by the O(1) vertex. The latter octahedron shares the O(2) vertex with the $[AsO_4]$ tetrahedron. This network gives rise to two kinds of chains, which are extended in perpendicular directions. Chain **1** is extended along the *a*-axis and it is constructed from F(2)–F(2) edge-sharing $[M^{II}(1)_2O_2F_8]$ (M = Mn, Co) dimmeric octahedra. Chain **2** runs along the *c*-axis and is formed by $[Fe^{III}(2)O_2F_4]$ octahedra and $[AsO_4]$ tetrahedra bonded between them through the O(2) atoms. These chains are linked by the F(1) and O(1) atoms and give rise to cavities

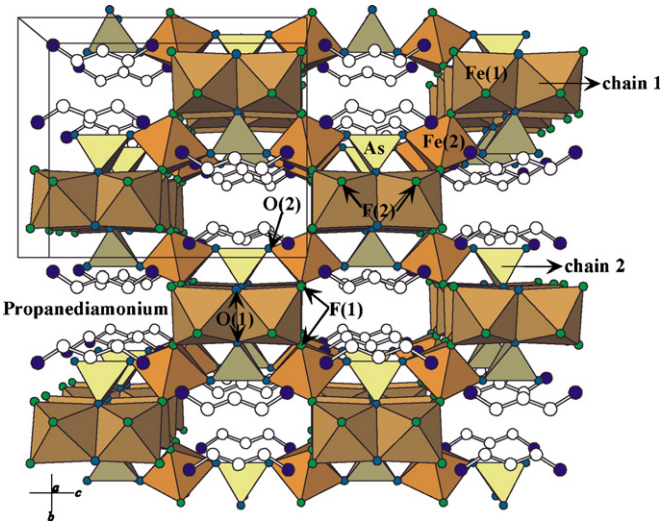

Fig. 3. Polyhedral representation of the crystal structure of compounds **1** and **2** along the [1 0 0] direction, showing the chains **1** and **2** and the cavities formed by eight polyhedra.

delimited by eight or six polyhedra along the [1 0 0] and [0 0 1] directions, respectively. The propanediammonium cations are located inside these cavities (Figs. 3 and 4). Fig. 5 displays a more detailed view of the chains for **1** and **2**.

3.2. Mössbauer spectroscopy

The Mössbauer spectrum in the paramagnetic state at 300 K has been fitted with the NORMOS program [10] using two doublets for the iron(III) cations, in accordance with the crystallographic results, which indicate the existence of two crystallographically independent positions for these cations. Taking into account the preferred orientation observed from X-ray powder diffraction measurements for compound **1**, the spectrum of this phase was recorded at 90° in respect to the gamma ray and at the *magic angle* of 55°. The results, given in Fig. 6, indicate very small preferred orientation manifested in the Mössbauer measurements, because the spectra are very similar. The best fits were obtained considering the simultaneous presence of the iron(III) cations in both the M(1) and M(2) positions for

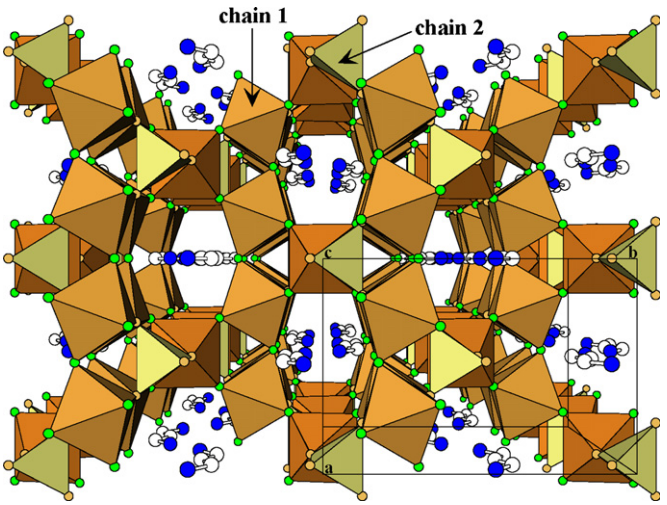

Fig. 4. Polyhedral representation of the crystal structure of compounds **1** and **2** along the [0 0 1] direction, showing the channels delimited by six polyhedra with the propanodiammonium cations.

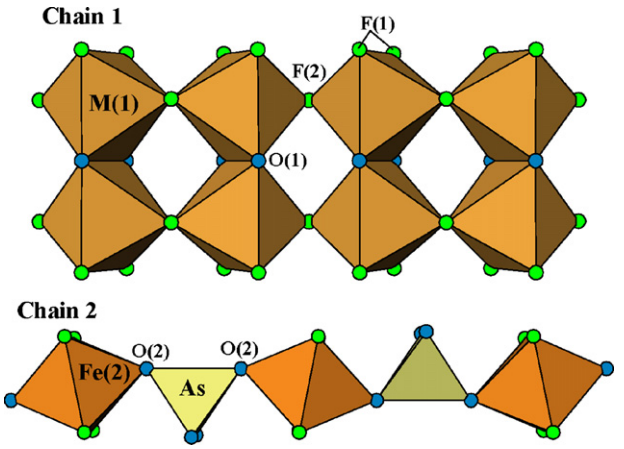

Fig. 5. View of the chains for **1** and **2**.

compounds **1** and **2** (see Fig. 6). The values of the isomer shift and quadrupolar splitting are given in Table 1, together with relative spectral area and the line-width associated to every doublet.

3.3. IR and UV–vis spectroscopy

The IR spectra of compounds **1** and **2** exhibit the bands corresponding to the vibrations of the water molecules, propanediammonium cations and the $[AsO_4]^{3-}$ oxoanions. The strong band centered at 3450 cm^{-1} corresponds to the stretching mode of the water molecules. The bending mode of these molecules can be observed at 1610 cm^{-1}. The stretching mode of the $(NH_3)^+$ group, in the propanediammonium cation, appears at 3000 cm^{-1}. The band near 1530 cm^{-1} can be assigned to the $(NH_3)^+$ bending vibration. This band is indicative of the presence of the propanediamine molecule in its protonated form [11] in good agreement with the structural results, which indicate that this molecule is not coordinated to the metallic cation. The bending vibrations of the $–CH_2–$ groups of the propanediammonium cation appear in the 1400–1200 cm^{-1} range. Three different groups of bands can be attributed to the vibrational modes of the $[AsO_4]^{3-}$ anions present in the compound [12]. The asymmetrical stretching mode [ν_{as}(As–O)] appears at the frequency of 820 cm^{-1}. The symmetrical stretch [ν_s(As–O)] is detected at a frequency of 760 cm^{-1}. The asymmetrical deformation vibration [δ_{as}(O–As–O)] can be observed about 470 cm^{-1}.

The diffuse reflectance spectra of the title compounds show several weak bands corresponding to the d^5 high spin Fe(III) and Mn(II) cations for compound **1**, and the spin allowed bands characteristic of the d^7 Co(II) cation in compound **2** (Fig. 7). The assignation of these bands, shown in Table 2, has been carried out taking into account the slightly distorted octahedral geometry, which exhibit the metallic cations in these phases.

Table 1
Values of the quadrupolar splitting (ΔE mm s^{-1}) and the isomer shift (δ mm s^{-1}) at room temperature for the compounds **1** and **2**

	Position	ΔE (mm s^{-1})	δ (mm s^{-1})	M.R.	Atoms per unit cell		% theoretical	% observed
Compound **1**	$Mn(1)^{2+}$	–	–	0.5	8	6	–	–
Angle = 90°	$Fe(1)^{3+}$	0.404	0.307			2	33.3	32
	$Fe(2)^{3+}$	0.417	0.475	0.25	4	4	66.6	68
Compound **1**	$Mn(1)^{2+}$	–	–	0.5	8	6	–	–
Magic Angle = 55°	$Fe(1)^{3+}$	0.402	0.336			2	33.3	39
	$Fe(2)^{3+}$	0.420	0.488	0.25	4	4	66.6	61
Compound **2**	$Co(1)^{2+}$	–	–	0.5	8	6	–	–
	$Fe(1)^{3+}$	0.394	0.320			2	33.3	32.3
	$Fe(2)^{3+}$	0.401	0.471	0.25	4	4	66.6	67.7

The values of the isomer shift, δ, and quadrupolar splitting, ΔE, are relatives to the α-Fe.

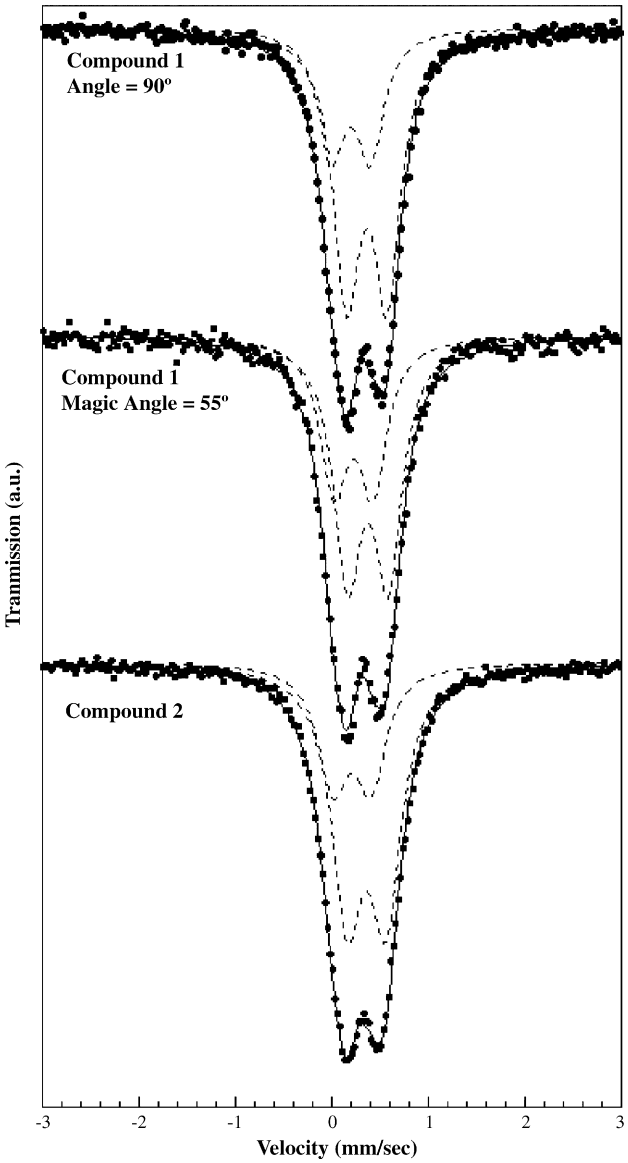

Fig. 6. Fit of the Mössbauer spectra.

The values of the Dq and B and C Racah parameters for the Fe(III) cation in compound **1** are 960, 955 and 2745 cm^{-1}, respectively, which are in good agreement with those given in the literature [13]. The *B* value is approximately 83% of that of the free Fe(III) ion (1150 cm^{-1}), indicating an appreciable degree of covalence in the Fe–O,F bonds. The presence of only two bands for the Mn(II) cation in compound **1** precludes calculating the Dq and Racah parameters. In compound **2**, the values obtained of the Dq and B-Racah parameters for the Co(II) ion are Dq = 710 and $B = 925$ cm^{-1}, in the range habitually found for these cations [13]. The *B* value is approximately 94% of that of the free Co(II) cation (971 cm^{-1}) which indicates a small degree of covalence in the Co–O,F bonds.

3.4. ESR behavior

The ESR spectra were registered at X-band from room temperature to 4.2 K (Fig. 8). The spectra of **1** exhibit an isotropic signal centered at 340 mT, resulting of the simultaneously existence in the compound of high spin d^5-Fe(III)

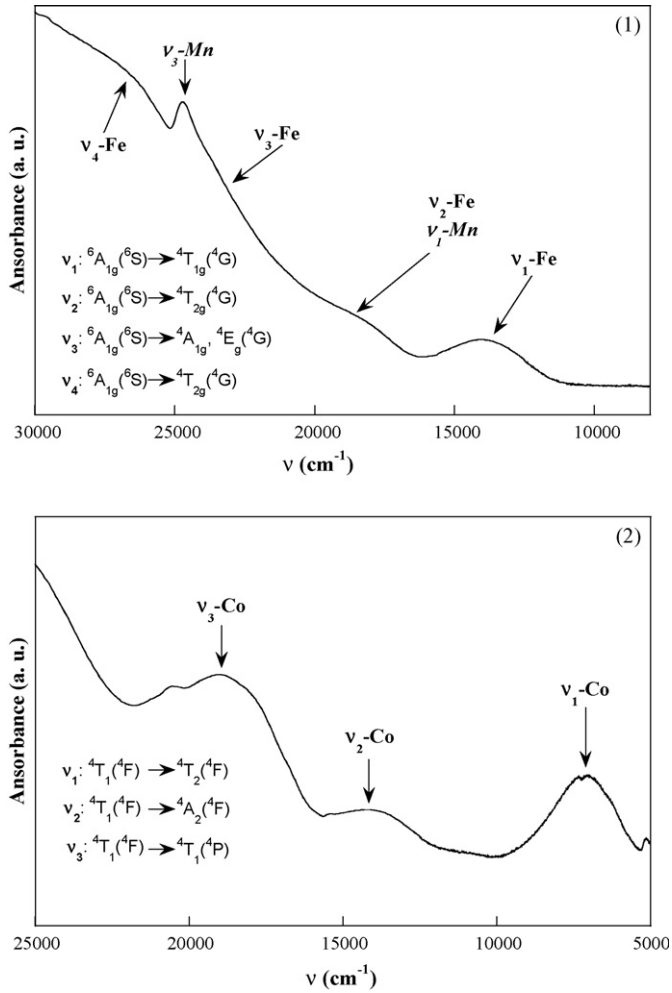

Fig. 7. Diffuse reflectance spectra for **1** and **2**.

Table 2
Assignation of the electronic transitions observed in the diffuse reflectace spectra of the compounds **1** and **2**

	Transition	Band (cm^{-1}), Fe^{3+} ion	Band (cm^{-1}), Mn^{2+} ion
Compound **1**			
ν_1	$^6A_{1g}(^6S) \rightarrow {}^4T_{1g}(^4G)$	13,940	18,400
ν_2	$^6A_{1g}(^6S) \rightarrow {}^4T_{2g}(^4G)$	18,400	–
ν_3	$^6A_{1g}(^6S) \rightarrow {}^4A_{1g}, {}^4E_g(^4G)$	23,280	24,695
ν_4	$^6A_{1g}(^6S) \rightarrow {}^4T_{2g}(^4G)$	26,145	–
ν_5	$^6A_{1g}(^6S) \rightarrow {}^4E_g(^4G)$	–	–
	Transition		Band (cm^{-1}), Co^{2+} ion
Compound **2**			
ν_1	$^4T_1(^4F) \rightarrow {}^4T_2(^4F)$		7,170
ν_2	$^4T_1(^4F) \rightarrow {}^4A_2(^4F)$		14,270
ν_3	$^4T_1(^4F) \rightarrow {}^4T_1(^4P)$		18,970

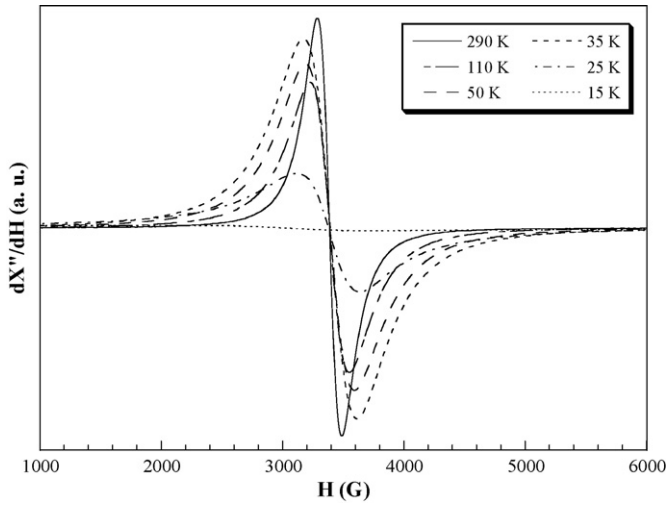

Fig. 8. ESR spectra at different temperatures for compound **1**.

and Mn(II) cations magnetically coupled. The ESR signals maintain practically unchanged from room temperature to 70 K. Below this temperature the signals broaden and loss intensity. The signals have been simulated using a Lorentzian curve, and then, the gyromagnetic *g*-tensor, the line-width and the intensity for every spectrum have been calculated. The value obtained for *g* is 1.99.

The thermal evolution of the line-width and intensity is given in Fig. 9. The intensity of the signals increases with decreasing temperature, showing a maximum at, approximately, 35 K. Below this temperature the intensity decreases dramatically. These results suggest the existence of antiferromagnetic couplings between the metallic centers. The line-width increases slowly in the 300–70 K range. Below this temperature an abrupt increase is observed probably due to a strong spin correlation [14]. The smaller value of the line-width observed in Fig. 7 at 10 K can be associated with an integration phenomenon.

In the ESR spectrum of **2** no signal was observed. This result is due to the low spin-relaxation time of the Co(II) cations, even at low temperature, which precludes observing the signal corresponding to the magnetically coupled Fe(III) cations.

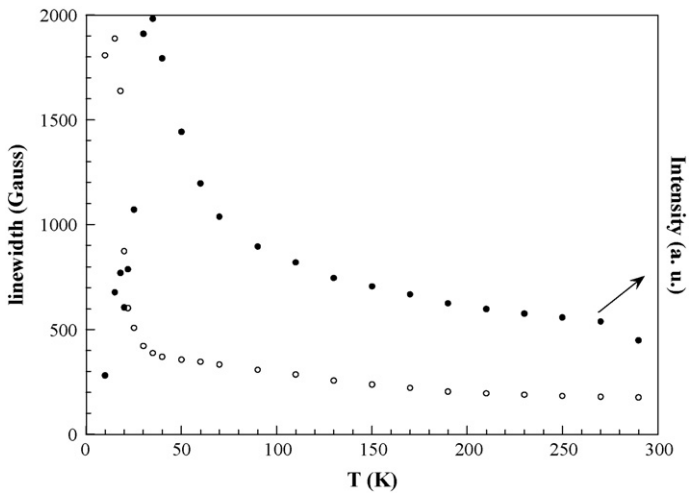

Fig. 9. Thermal evolution of the line-width and intensity of the ESR signals of **1**.

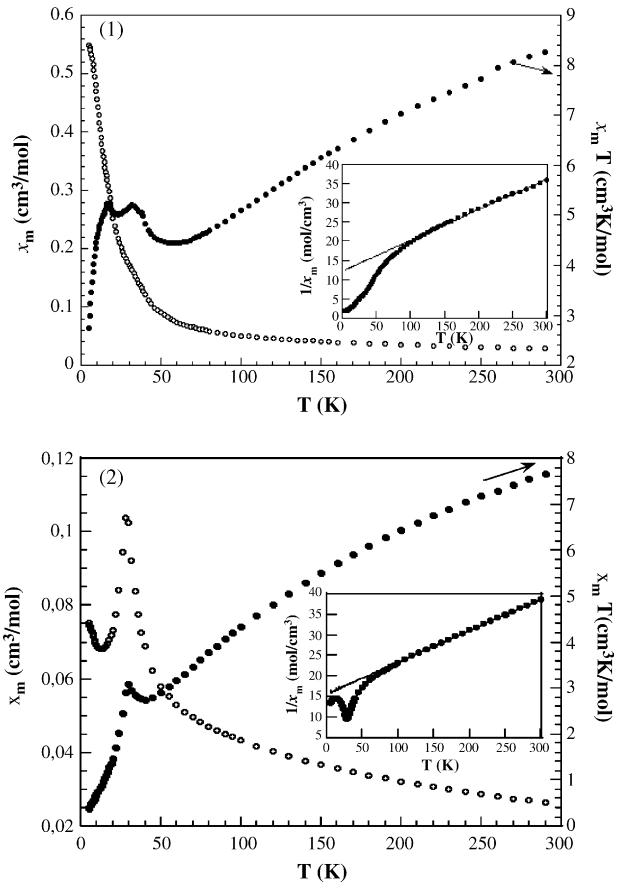

Fig. 10. χ_m and $\chi_m T$ *vs.* T curves carried out at 0.1 T for **1**.

3.5. Magnetic behavior

Variable-temperature magnetic measurements of the compounds **1** and **2** have been performed at values of the magnetic field de 0.1, 0.05 and 0.01 T in the ZFC (*zero field cooling*) and FC (*field cooling*) modes. The χ_m and $\chi_m T$ *versus* T curves carried out at 0.1 T are shown in Fig. 10. The compounds follow a Curie–Weiss law a temperatures higher than 100 K for **1** and **2**, respectively (see inset in Fig. 10). The Curie constant and Weiss temperature are 12.55 cm^3 K/mol, −154.4 K for **1** and 13.02 cm^3 K/mol, −204.4 K for **2**. The deviation of the Curie constant for **2**, 13.02 cm^3 K/mol *versus* 12.10 cm^3 K/mol, this later evaluated from the spin only contribution considering $g \cong 2.2$ for Co(II) [15], is probably due to the orbital contribution of the Co(II) cation, which makes not possible to calculate the exact value of the g-factor for this cation. The effective magnetic moments at room temperature, $\mu_{eff.}$, are 10.02 BM for **1** [approximately, 5.0 BM for each cation, Mn(II) and Fe(III), according to the stoichiometry of the chemical formula] and 10.20 BM for **2**. The difficulty to evaluate the orbital contribution of the Co(II) metallic cation to the $\mu_{eff.}$, it makes not possible to know the individual contribution of Fe(III) and Co(II) to this one, for compound **2**.

The molar magnetic susceptibility of **1** increases continuously in all the temperature range studied. The $\chi_m T$ *versus* T curve decreases continuously from room temperature down to 55 K (see Fig. 9). Below this temperature the curve exhibits a small maximum, which can be associated with a weak ferromagnetic contribution, probably due to a spin decompensation between the Mn(II) and Fe(III) cations. The second maximum is detected at around 25 K, probably due to a magnetic impurity. Finally, this curve decreases down to 2.61 cm^3 K/mol at 5 K. These results confirm that the main magnetic interactions are antiferromagnetic in nature. However the increase observed in the $\chi_m T$ *versus* T curve at 50 K suggests the existence of a weak ferromagnetic contribution that takes place in a small temperature range. This way, the susceptibility measurements carried out at 0.1 and 0.05 T in the ZFC and FC modes show irreversibility, being the separation between the curves greater when the magnetic field decreases (Fig. 11).

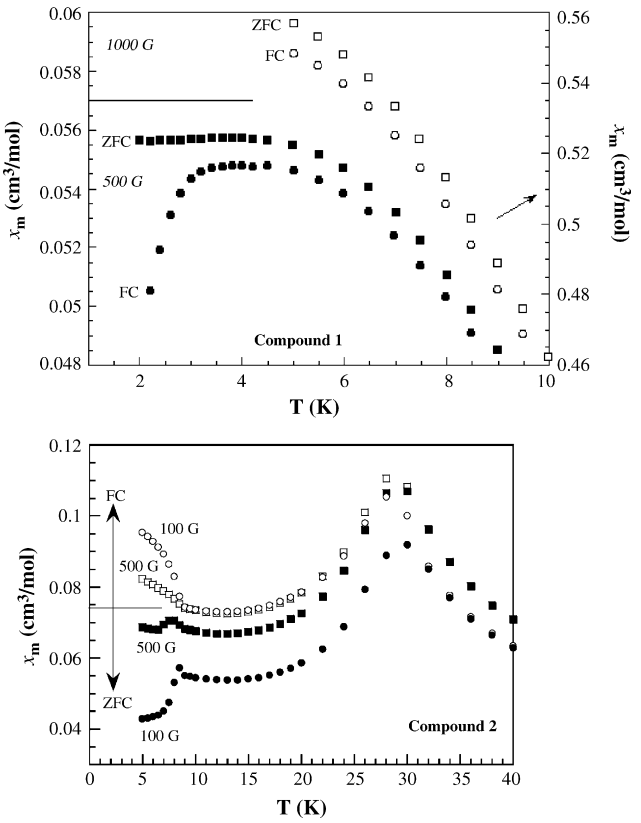

Fig. 11. Thermal evolution of the χ_m and $\chi_m T$ *vs. T* curves collected at 0.05 and 0.01 T for **2**, showing their irreversibility.

For compound **2**, the thermal evolution of the molar magnetic susceptibility performed at 0.1 T is shown in Fig. 10. The susceptibility increases continuously from room temperature up to 28 K, temperature at which a sharp maximum is observed, probably three-dimensional in nature due to the structural features of this phase. Below 28 K the susceptibility decreases down to 14 K, and finally a small increase is observed, probably due to a paramagnetic impurity. The $\chi_m T$ *versus T* curve decreases continuously from room temperature down to 30 K, temperature at which a sharp maximum is observed. Below this temperature the curve decreases down to 5 K. Both, the maximum observed in χ_m *versus T* curve and the decrease of the $\chi_m T$ product indicate that the main interactions are antiferromagnetic, though the continuous decrease of the $\chi_m T$ curve with decreasing temperature must also be ascribed to the effect of the spin–orbit coupling ($\lambda = -170$ cm^{-1} for free Co(II) ion) [16] which leads to an effective spin of $S = 1/2$ for the system at low temperatures (<30 K). This latter effect is qualitatively similar to those of the antiferromagnetic interactions, making it difficult to distinguish the contributions of these two effects to the whole magnetic behavior of this compound. On the other hand, the maximum observed in the $\chi_m T$ *versus T* curve suggests the existence of a ferromagnetic component at low temperature. Similarly to that found for compound **1**, the susceptibility measurements of **2** carried out at 0.05 and 0.01 T in the ZFC and FC modes show irreversibility, being the separation between the curves greater when the magnetic field decreases (see Fig. 11).

In order to confirm the weak ferromagnetic contributions observed in both, phases **1** and **2**, magnetization measurements as function of the magnetic field were carried out at 5 K. Hysteresis loops were obtained with values of the remnant magnetization and the coercive field of 84.5 emu/mol, 10^{-2} T and 255 emu/mol, 0.225 T, for **1** and **2**, respectively (see Fig. 12).

Taking into account the structural features of these 3D-compounds in which the framework is formed by two kinds of perpendicular chains (see Fig. 13), several magnetic exchange pathways can take place: (i) direct intradimeric antiferromagnetic interactions inside the $M(1)_2O_2F_8$ [M = Mn(II), Co(II)] dimeric units involving the $d_x2_{-y}2$ orbitals from the M(1) cations, (ii) superexchange pathways through the O(1), F(1) and F(2) atoms which are linked to the

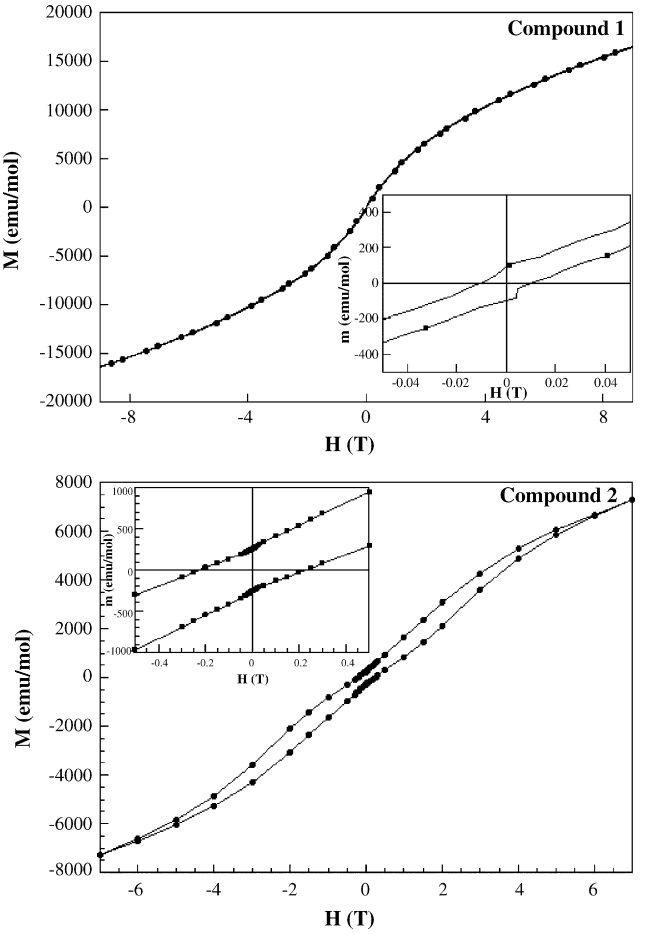

Fig. 12. Hysteresis loops at 5.0 K for **1** and **2**.

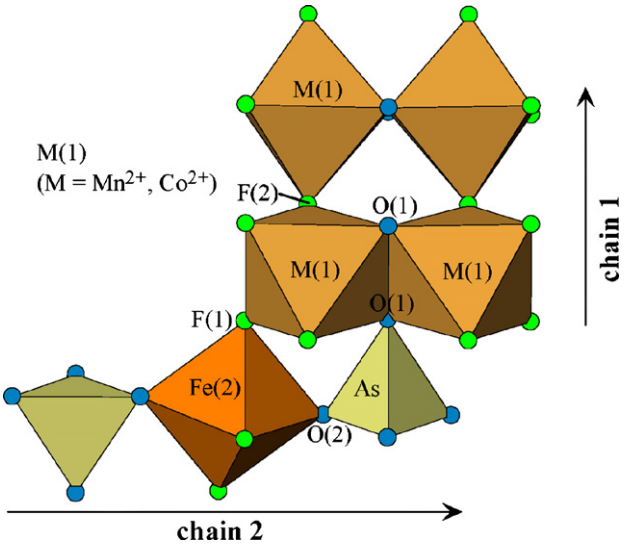

Fig. 13. Polyhedral representation of the possible magnetic exchange pathways.

metallic cations. The values of the involved M(1)–O(1)–M(1), M(1)–F(2)–M(1) and Fe(2)–F(1)–M(1) must be near to 90° for M(1)–O(1)–M(1) and to 130° for the other M(1)–F(2)–M(1) and Fe(2)–F(1)–M(1) bond angles, as was observed in the isostructural $(C_3H_{12}N_2)_{0.75}[Fe_{1.5}^{II}Fe_{1.5}^{III}(AsO_4)F_6]$ [7]. The value of the bond angle for the first pathway [M(1)–O(1)–M(1)] could originate a ferromagnetic interaction [17] inside the $M(1)_2O_2F_8$ dimers, belonging to chain **2**. Nonetheless, the bond angles for the other two superexchange pathways [M(1)–F(2)–M(1), Fe(2)–F(1)–M(1)] clearly indicate the existence of antiferromagnetic interactions in chain **1** along the [1 0 1] direction [17], (iii) finally, superexchange interactions through the $[AsO_4]^{3-}$ anions linking the metallic octahedra, that favor the antiferromagnetic couplings take place [17].

4. Concluding remarks

Two new isostructural mixed valent metallic fluoro-arsenates organically templated with the diaminopropane molecule have been synthesized using mild hydrothermal conditions. The crystal structures consist of a three-dimensional inorganic framework constructed from two kinds of perpendicular chains. The propanediammonium cations are located inside the cavities delimited for the chains. The thermal analysis indicates that the crystal structures collapse with calcination of the organic dications. The spectroscopy in the visible region indicates the existence of the divalent manganese(II) and cobalt(II) cations and the iron(III) ions in a slightly distorted octahedral symmetry. Mössbauer measurements show a small substitution of the divalent cations by the trivalent iron(III) ions. The ESR spectra of the manganese(II)–iron(III) phase are isotropic with the metallic cations magnetically coupled. Magnetic measurements show that the main magnetic couplings are antiferromagnetic in nature. At low temperatures weak ferromagnetic interactions are detected, probably caused by a spin decompensation between the different paramagnetic metallic cations.

Acknowledgements

This work has been financially supported by the ‘‘Ministerio de Educación y Ciencia’’ (MAT2004-0271) and the ‘‘Universidad del País Vasco’’ (UPV/EHU) (9/UPV00130.310-13700/2001) and (9/UPV00169.310-13494/2001). B. Bazan thanks to the UPV/EHU for funding.

Appendix A. Supplementary data

Supplementary data associated with this article can be found, in the online version, at doi:10.1016/j.materresbull.2007.05.016.

References

[1] M.E. Davis, Chem. Eur. 3 (1997) 1745.
[2] (a) A.K. Cheetham, G. Ferey, T. Loisseau, Angew, Chem. Int. Ed. Engl. 38 (1999) 3268;
(b) A. Choudhury, S. Natarajan, C.N.R. Rao, J. Solid State Chem. 146 (1999) 538;
(c) M.R. Cavellec, D. Riou, G. Ferey, Inorg. Chim. Acta 291 (1999) 317.
[3] (a) J. Escobal, J.L. Pizarro, J.L. Mesa, L. Lezama, R. Olazcuaga, M.I. Arriortua, T. Rojo, Chem. Mater. 12 (2000) 376;
(b) J.R.D. DeBord, W.M. Reiff, C.J. Warren, R. Haushalter, J. Zubieta, Chem. Mater. 9 (1997) 1994;
(c) J.R.D. DeBord, W.M. Reiff, R. Haushalter, J. Zubieta, J. Solid State Chem. 125 (1996) 186.
[4] (a) M. Cavellec, D. Riou, C. Ninclaus, J.M. Greneche, G. Ferey, Zeolites 17 (1996) 250;
(b) M. Cavellec, D. Riou, J.M. Greneche, G. Ferey, Inorg. Chem. 36 (1997) 250;
(c) K.H. Lii, Y.F. Huang, J. Chem. Soc., Chem. Commun. 1311 (1997);
(d) V. Zima, K.H. Lii, N. Nguyen, A. Ducouret, Chem. Mater. 10 (1998) 1914;
(e) K.H. Lii, Y.F. Huang, J. Chem. Soc., Dalton Trans. 2221 (1997);
(f) M. Cavellec, C. Eger, L. Linares, N. Nogues, F. Barret, G. Ferey, J. Solid State Chem. 134 (1997) 349;
(g) M. Riou-Cavellec, D. Riou, G. Ferey, Inorg. Chim. Acta 291 (1999) 317;
(h) A. Choudhury, S. Narajan, J. Solid State Chem. 154 (2000) 507;
(i) S. Mandal, S. Natarajan, J.M. Grneche, M. Riou-Cavellec, G. Ferey, Chem. Mater. 14 (2002) 3751.
[5] (a) H. Kesler, Stud. Sci. Catal. 52 (1989) 17;
(b) G. Ferey, T. Loisseau, D. Riou, Advanced Inorganic Fluorides: Synthesis, Characterization and Applications, Elsevier Science, New York, 2000, chapter 7, p. 207.

[6] (a) S. Ekambarm, S.C. Sevoc, Inorg. Chem. 39 (2000) 2405;
(b) Y.C. Liao, S.H. Luo, S.L. Wang, H.M. Kao, K.H. Lii, J. Solid State Chem. 155 (2000) 37;
(c) B. Bazan, J.L. Mesa, J.L. Pizarro, L. Lezama, M.I. Arriortua, T. Rojo, Inorg. Chem. 39 (2000) 6056;
(d) S.H. Luo, Y.C. Jiang, S.L. Wang, H.M. Kao, K.H. Lii, Inorg. Chem. 40 (2001) 5381;
(e) B. Bazan, J.L. Mesa, J.L. Pizarro, A. Goñi, L. Lezama, M.I. Arriortua, T. Rojo, Inorg. Chem. 40 (2001) 5691;
(f) S. Chakrabarti, M.A. Green, S. Natarajan, Solid State Sci. 4 (2000) 405;
(g) B. Bazan, J.L. Mesa, J.L. Pizarro, J.S. Garitaonandia, M.I. Arriortua, T. Rojo, Solid State Sci. 5 (2003) 1291;
(h) B. Bazan, J.L. Mesa, J.L. Pizarro, M.I. Arriortua, T. Rojo, Mater. Res. Bull. 39 (2003) 1193.
[7] B. Bazan, J.L. Mesa, J.L. Pizarro, A. Peña, M.I. Arriortua, T. Rojo, Z. Anorg. Allg. Chem. 631 (2005) 2026.
[8] (a) Powder Diffraction File, Inorganic and Organic, 21-910;
(b) Powder Diffraction File, Inorganic and Organic, 39-1346;
(c) Powder Diffraction File, Inorganic and Organic, 81-2060;
(d) Powder Diffraction File, Inorganic and Organic, 82-2169;
(e) Powder Diffraction File, Inorganic and Organic, 77-1745;
(f) Powder Diffraction File, Inorganic and Organic, 48-1719.
[9] J. Rodriguez-Carvajal, FULLPROF Program, Rietveld Pattern Matching Análisis of Powder Patterns, Unpublished Results, 1994.
[10] R.A. Brand, J. Larner, D.M. Herlach, J. Phys. F14 (1984) 555.
[11] A. Gharbi, A. Jouini, M.T. Averbuch-Pouchot, A. Durif, J. Solid State Chem. 111 (1994) 330.
[12] K. Nakamoto, Infrared and Raman Spectroscopy of Inorganic and Coordination Compounds, John Wiley & Sons, New York, 1997.
[13] A.B.P. Lever, Inorganic Electronic Spectroscopy, Elsevier Science Publisher, B.V., Amsterdam, Netherlands, 1984.
[14] (a) H.W. Wijn, L.R. Wlaker, J.L. Daris, H.J. Guggenheim, Solid State Commun. 11 (1972) 803;
(b) P.M. Richards, M.B. Salomon, Phys. Rev. B 9 (1974) 32;
(c) A. Escuer, R. Vicente, M.A.S. Goher, F. Mautner, Inorg. Chem. 34 (1995) 5707;
(d) A. Bencini, D. Gatteschi, EPR of Exchange Coupled Systems, Springer-Verlag, Berlin, 1990;
(e) T.T.P. Cheung, Z.G. Soos, R.E. Dietz, F.R. Merrit, Phys. Rev. B 17 (1978) 1266.
[15] R.L. Carlin, Magnetochemistry, Springer-Verlag, Berlin, 1986.
[16] T.M. Dunn, Trans. Faraday Soc. 57 (1961) 1441.
[17] J.B. Goodenough, Magnetism and the Chemical Bond, Interscience, New York, 1963.